Check for updates

Electromagnetic behavior of dielectric objects on metallic periodically nanostructured substrates

Á. I. BARREDA,[1] D. OTADUY,[2] R. MARTÍN-RODRÍGUEZ,[3,4] S. MERINO,[2] J. L. FERNÁNDEZ-LUNA,[5] F. GONZÁLEZ,[1] AND F. MORENO[1,*]

[1]*Department of Applied Physics, Univ. of Cantabria, Avda. Los Castros s/n, 39005 Santander, Spain*
[2]*IK4-TEKNIKER, C/ Iñaki Goenaga 5, 20600 Eibar, Spain*
[3]*QUIPRE Department, Univ. of Cantabria, Avda. Los Castros s/n, 39005 Santander, Spain*
[4]*Nanomedicine Group, IDIVAL, Avda. Cardenal Herrera Oria s/n, 39011 Santander, Spain*
[5]*Unidad de Genética, HUMV, Avda. Marqués de Valdecilla s/n, 39008 Santander, Spain*
[*]*morenof@unican.es*

Abstract: In this research, we investigate the electromagnetic behavior of a metallic thin-film with a periodic array of subwavelength apertures when dielectric objects are located on it. The influence of size, geometry and optical properties of the objects on the transmission spectra is numerically analyzed. We study the sensitivity of this system to changes in the refractive index of the illuminated volume induced by the presence of objects with sizes from hundreds of nanometers (submicron-sized objects) to a few microns (micron-sized objects). Parameters such as the object volume within the penetration depth of the surface plasmon in the buffer medium or the contact surface between the object and the nanostructured substrate strongly affect the sensitivity. The proposed system models the presence of objects and their detection through the spectral shifts undergone by the transmission spectra. Also, we demonstrate that these can be used for obtaining information about the refractive index of a micron-sized object immersed in a buffer and located on the nanostructured sensitive surface. We believe that results found in this study can help biomedical researchers and experimentalists in the process of detecting and monitoring biological organisms of large sizes (notably, cells).

References and links

1. T. Thio, H. J. Lezec, T. W. Ebbesen, K. M. Pellerin, G. D. Lewen, A. Nahata, and R. A. Linke, "Giant optical transmission of sub-wavelength apertures: physics and applications," Nanotechnology **13**, 429–432 (2002).
2. T. W. Ebbesen, H. J. Lezec, H. F. Ghaemi, T. Thio, and P. A. Wolff, "Extraordinary optical transmission through sub-wavelength hole arrays," Nature **391**, 667–669 (1998).
3. H. F. Ghaemi, T. Thio, D. E. Grupp, T. W. Ebbesen, and H. J. Lezec, "Surface plasmons enhance optical transmission through subwavelength holes," Phys. Rev. B **58**(11), 6779–6782 (1998).
4. A. Lesuffleur, H. Im, N. C. Lindquist, and S.-H. Oh, "Periodic nanohole arrays with shape-enhanced plasmon resonance as real-time biosensors," Appl. Phys. Lett. **90**(24), 243110 (2007).
5. J. S. Kee, S. Lim, A. P. Perera, and M. K. Park, "Plasmonic Nanohole Array for Biosensor Applications," in Proceedings of IEEE Photonics Global Conference (IEEE, 2012), pp. 1–4.
6. R. Gordon, A. G. Brolo, D. Sinton, and K. L. Kavanagh, "Resonant optical transmission through hole-arrays in metal films: physics and applications," Laser Photon. Rev. **4**(2), 311–335 (2010).
7. M. Shioi, H. Jans, K. Lodewijks, P. Van Dorpe, L. Lagae, and T. Kawamura, "Tuning the interaction between propagating and localized surface plasmons for surface enhanced Raman scattering in water for biomedical and environmental applications," Appl. Phys. Lett. **104**(24), 243102 (2014).
8. M. Couture, Y. Liang, H.-P. Poirier Richard, R. Faid, W. Peng, and J.-F. Masson, "Tuning the 3D plasmon field of nanohole arrays," Nanoscale **5**(24), 12399–408 (2013).
9. M. Couture, L. S. Live, A. Dhawan, and J.-F. Masson, "EOT or Kretschmann configuration? Comparative study of the plasmonic modes in gold nanohole arrays," Analyst **137**(18), 4162–4170 (2012).

10. J. Le Perchec, P. Quémerais, A. Barbara, and T. López-Ríos, "Why Metallic Surfaces with Grooves a Few Nanometers Deep and Wide May Strongly Absorb Visible Light," Phys. Rev. Lett. **100**(6), 066408 (2008).

11. S. M. Jang, D. Kim, S. H. Choi, K. M. Byun, and S. J. Kim, "Enhancement of localized surface plasmon resonance detection by incorporating metal-dielectric double-layered subwavelength gratings," Appl. Opt. **50**(18), 2846–2854 (2011).

12. J. Homola, "Present and future of surface plasmon resonance biosensors," Anal. Bioanal. Chem. **377**(3), 528–539 (2003).

13. J. Zhang, L. Zhang, and W. Xu, "Surface plasmon polaritons: physics and applications," J. Phys. D: Appl. Phys. **45**(11), 113001 (2012).

14. A. G. Brolo, "Plasmonics for future biosensors," Nat. Photonics **6**, 709–713 (2012).

15. J. C. M. Wan, C. Massie, J. García-Corbacho, F. Mouliere, J. D. Brenton, C. Caldas, S. Pacey, R. Baird, and N. Rosenfeld, "Liquid biopsies come of age: towards implementation of circulating tumour DNA," Nat. Rev. Cancer **17**, 223–238 (2017).

16. R. Gordon, D. Sinton, K. L. Kavanagh, and A. G. Brolo, "A New Generation of Sensors Based on Extraordinary Optical Transmission," Acc. Chem. Res. **41**(8), 1049–1057 (2008).

17. G. A. Cervantes Tellez, S. Hassan, R. N. Tait, P. Berini, and R. Gordon, "Atomically flat symmetric elliptical nanohole arrays in a gold film for ultrasensitive refractive index sensing," Lab Chip **13**(13), 2541–2546 (2013).

18. T. I. Wong, S. Han, L. Wu, Y. Wang, J. Deng, C. Y. L. Tan, P. Bai, Y. C. Loke, X. D. Yang, M. S. Tse, S. H. Ng, and X. Zhou, "High throughput and high yield nanofabrication of precisely designed gold nanohole arrays for fluorescence enhanced detection of biomarkers," Lab Chip **13**(12), 2405–2413 (2013).

19. P. Y. Liu, L. K. Chin, W. Ser, H. F. Chen, C.-M. Hsieh, C.-H. Lee, K.-B. Sung, T. C. Ayi, P. H. Yap, B. Liedberg, K. Wang, T. Bourouina, and Y. Leprince-Wang, "Cell refractive index for cell biology and disease diagnosis: past, present and future," Lab Chip **16**(4), 634–644 (2016).

20. E. M. Ortiz, P. J. Valle, J. M. Saiz, F. González, and F. Moreno, "A detailed study of the scattered near field of nanoprotuberances on flat surfaces," J. Phys. D: Appl. Phys. **31**(21), 3009–3019 (1998).

21. E. M. Ortiz, P. J. Valle, J. M. Saiz, F. González, and F. Moreno, "Multiscattering effects in the far-field region for two small particles on a flat conducting substrate," Waves Random Media **7**(3), 319–329 (1997).

22. F. Moreno, B. García-Cámara, J. M. Saiz, and F. González, "Interaction of nanoparticles with substrates: effects on the dipolar behaviour of the particles," Opt. Express **16**(17), 12487–12504 (2008).

23. J. L. de la Peña, F. González, J. M. Saiz, F. Moreno, and P. J. Valle, "Sizing particles on substrates. A general method for oblique incidence," J. Appl. Phys. **85**(1), 432–438 (1999).

24. J. L. de la Peña, J. M. Saiz, G. Videen, F. González, P. J. Valle, and F. Moreno, "Scattering from particles on surfaces: visibility factor and polydispersity," Opt. Lett. **24**(21), 1451–1453 (1999).

25. J. M. Saiz, P. J. Valle, F. González, E. M. Ortiz, and F. Moreno, "Scattering by a metallic cylinder on a substrate: burying effects," Opt. Lett. **21**(17), 1330–1332 (1996).

26. P. J. Valle, F. González, and F. Moreno, "Electromagnetic wave scattering from conducting cylindrical structures on flat substrates: study by means of the extinction theorem," Appl. Opt. **33**(3), 512–523 (1994).

27. F. Moreno, J. M. Saiz, P. J. Valle, and F. González, "Metallic particle sizing on flat surfaces: Application to conducting substrates," Appl. Phys. Lett. **68**(22), 3087–3089 (1996).

28. J. M. Saiz, P. J. Valle, F. González, F. Moreno and D. L. Jordan, "Backscattering from particulate surfaces: experiment and theoretical modeling," Opt. Eng. **33**(4), 1261–1270 (1994).

29. P. J. Valle, F. Moreno, J. M. Saiz, and F. González, "Electromagnetic interaction between two parallel circular cylinders on a planar interface," IEEE Trans. Antennas Propag. **44**(3), 321–325 (1996).

30. F. González, J. M. Saiz, P. J. Valle, and F. Moreno, "Multiple scattering in particulate surfaces: Cross-polarization ratios and shadowing effects," Opt. Commun. **137**, 359–366 (1997).

31. E. Baquedano, M. U. González, R. Paniagua-Domínguez, J. A. Sánchez-Gil and P. A. Postigo, "Low-cost and large-size nanoplasmonic sensor based on Fano resonances with fast response and high sensitivity," Opt. Express **25**(14), 15967–15976 (2017).

32. B. Zeng, Y. Gao and F. J. Bartoli, "Rapid and highly sensitive detection using Fano resonances in ultrathin plasmonic nanogratings," Appl. Phys. Lett. **105**(16), 161106 (2014).

33. K. D. Young, "Bacterial morphology: Why have different shapes?" Curr. Opin. Microbiol. **10**(6), 596–600 (2007).

34. A. Tripathy, P. Sen, B. Su, W. H. Briscoe, "Natural and bioinspired nanostructured bactericidal surfaces," Adv. Colloid Interface Sci. **248**, 85–104 (2017).

35. S. Vinjimore Kesavan, F. Momey, O. Cioni, B. David-Watine, N. Dubrulle, S. Shorte, E. Sulpice, D. Freida, B. Chalmond, J. M. Dinten, X. Gidrol, and C. Allier, "High-throughput monitoring of major cell functions by means of lensfree video microscopy," Sci. Rep. **4**, 5942 (2014).

36. A. Yanik, A. E. Cetin, M. Huang, A. Artar, S. H. Mousavi, A. Khanikaev, J. H. Connor, G. Shvets, and H. Altug, "Seeing protein monolayers with naked eye through plasmonic fano resonances," Proc. Natl. Acad. Sci. U.S.A. **108**(29), 11784–11789 (2011).

37. H. Raether, *Surface Plasmons on Smooth and Rough Surfaces and on Gratings* (Springer Berlin Heidelberg, 1988).

38. R. Zia, M. D. Selker, and M. L. Brongersma, "Leaky and bound modes of surface plasmon waveguides," Phys. Rev. B **71**(16), 165431 (2005).

39. C. Genet and T. W. Ebbesen, "Light in tiny holes," Nature **445**, 39–46 (2007).

40. A. Djalalian-Assl, J. J. Cadusch, Z. Q. Teo, T. J. Davis, and A. Roberts, "Surface plasmon wave plates," Appl. Phys. Lett. **106**(4), 041104 (2015).
41. E.D. Palik, *Handbook of Optical Constants of Solids* (Academic, 1998).
42. COMSOL Multiphysics 5.0, *COMSOL Inc.* (http://www.comsol.com/).
43. J. Martinez-Perdiguero, A. Retolaza, A. Juarros, D. Otaduy, and S. Merino, "Enhanced Transmission through Gold Nanohole Arrays Fabricated by Thermal Nanoimprint Lithography for Surface Plasmon Based Biosensors," Procedia Eng. **47**, 805–808 (2012).
44. J. Martinez-Perdiguero, A. Retolaza, D. Otaduy, A. Juarros, and S. Merino, "Real-Time Label-Free Surface Plasmon Resonance Biosensing with Gold Nanohole Arrays Fabricated by Nanoimprint Lithography," Sensors **13**(10), 13960–13968 (2013).
45. P. Albella, F. Moreno, J. M. Saiz, and F. González, "Monitoring small defects on surface microstructures through backscattering measurements," Opt. Lett. **31**(11), 1744–1746 (2006).
46. P. Albella, F. Moreno, J. M. Saiz, and F. González, "Backscattering of metallic microstructures with small defects located on flat substrates," Opt. Express **15**(11), 6857–6867 (2007).
47. A. Colombelli, M. G. Manera, G. Montagna, R. Rella, and A. Convertino, "Three-dimensional Plasmonic Materials for Chemical Sensor Application," in Proceedings of the Second National Conference on Sensors, D. Compagnone, F. Baldini, C. Di Natale, G. Betta, and P. Siciliano, eds. (Switzerland: Springer International Publishing, 2015), pp. 171–175.
48. X. Cui, K. Tawa, K. Kintaka, and J. Nishii, "Enhanced Fluorescence Microscopic Imaging by Plasmonic Nanostructures: From a 1D Grating to a 2D Nanohole Array," Adv. Funct. Mater. **20**(6), 945–950 (2010).
49. M. E. Abdelsalam, P. N. Bartlett, T. Kelf, and J. Baumberg, "Wetting of regularly structured gold surfaces," Langmuir **21**(5), 1753–1757 (2005).
50. A. E. Cetin, D. Etezadi, B. C. Galarreta, M. P. Busson, Y. Eksioglu, and H. Altug, "Plasmonic Nanohole Arrays on a Robust Hybrid Substrate for Highly Sensitive Label-Free Biosensing," ACS Photonics **2**(8), 1167–1174 (2015).
51. J. P. Monteiro, L. B. Carneiro, M. M. Rahman, A. G. Brolo, M. J. L. Santos, J. Ferreira, and E. M. Girotto, "Effect of periodicity on the performance of surface plasmon resonance sensors based on subwavelength nanohole arrays," Sens. Actuator. B Chem. **178**, 366–370 (2013).
52. W. J. Choi, D. I. Jeon, S. G. Ahn, J. H. Yoon, S. Kim and B. H. Lee, "Full-field optical coherence microscopy for identifying live cancer cells by quantitative measurement of refractive index distribution," Opt. Express **18**(22), 23285–23295 (2010).

1. Introduction

Nanotechnology has revolutionized science over the last years. In particular, the interaction of electromagnetic radiation with metals at the nanometric scale has opened a new research field. In presence of electromagnetic radiation, free electrons in the metal oscillate with the same frequency as the incident radiation, giving rise to surface plasmons (SP's). These are called localized (LSP's) when this phenomenon occurs in metallic nanoparticles. At certain frequencies of the incident radiation, these oscillations resonate, leading to resonant surface plasmons (localized for nanoparticles)

Following diffraction theory, in 1944 Bethe theoretically predicted that transmission through a circular subwavelength hole (normalized to its area) perforated in an infinitely thin perfect conductor film was directly (inversely) related to the fourth power of radius (wavelength of incident light) [1]. However, experimental results were not consistent with such theoretical predictions [2]. In particular, when incident light goes through a periodic array of subwavelength apertures perforated in a metallic thin-film, resonance peaks are clearly observed in the transmission spectra. These resonances constitute what is known as the Extraordinary Optical Transmission (EOT) phenomenon, where surface plasmons (SP's) play an important role [2, 3].

SP's are inhomogeneous waves which appear at the interface between two media with opposite sign in the real part of their permittivity, for instance, at the interface of a dielectric and a metal. This is also the case of a metallic thin-film (tens of nanometers) perforated with a periodic array of subwavelength apertures, sandwiched between two dielectric media, one acting as a supporting substrate (usually glass) and the other as a medium (buffer + "contaminant" material) whose optical properties are of interest. In this situation, the electromagnetic radiation is confined in the proximities of the metallic surface and propagating through it in form of evanescent waves.

Since the excitation wavelength of the SP's strongly depends on the dielectric constant of

both the dielectric medium to be sensed and the metallic thin-film, small changes in the optical properties of the dielectric medium manifest as spectral shifts of the position of the transmission resonances. This is one of the main reasons why plasmonic metallic nanostructures have been vastly investigated and proposed for applications in label-free biosensing, polarization control, filtering, switching, nonlinear optics, Surface-Enhanced Fluorescence, Surface-Enhanced Raman scattering and absorption spectroscopy [4–7]. In particular, they are ideal "nano-tools" for detecting low concentrations of biological material, usually with sizes smaller than the incident wavelength. In such case, it is important that the material is close enough to the dielectric-metal interface so that it is inside the penetration depth of the plasmon in the buffer [8–14].

Many previous studies aiming to detect biological material located on a periodic array of subwavelength metallic apertures draw on to effective medium theories in order to determine the optical properties of the composite made by the buffer and the biological material [12]. In general, the interest lies in detecting biological components whose size is in the nanometric range: proteins, viruses, rests of RNA, etc. With the recent advances in liquid biopsies for diagnosis purposes, biological objects whose size is in the micrometric range have to be considered (cells, for instance) [15]. In particular, a blood sample is flowed through a microfluidic system built on a nanostructured surface which has been previously biofuncionalized. Due to specific antibodies (usually, EpCam), cells can be trapped on the surface of the nanostructured substrate [6, 14, 16–18]. The measurement of the spectral shifts of plasmonic resonances allows to detect the presence of biological organisms or even count them (cells for instance) and to obtain information about its optical properties. Furthermore, it has been recently demonstrated that refractive index is an important optical factor to distinguish between cells of different nature. In general, cancer cells show a global refractive index higher than that of healthy cells [19]. Many works dealing with light scattering of micron-sized objects on flat substrates have revealed how the optical presence of these objects alter the electromagnetic response of the substrates where they are located [20–30]. In this work, we study the electromagnetic response of the nanostructured system when the buffer contains objects with sizes ranging from hundreds of nanometers (submicron-sized objects) to microns (micron-sized objects). Even for submicron-sized objects, the considered sizes are larger than those usually detected by using sensors based on LSP's [31, 32], which are smaller than tens of nanometers.

A detailed study is performed as follows: Section 2 briefly reviews the theoretical background. Section 3 shows the most important results. In particular, Section 3.1 is devoted to study the spectral shifts in the transmission spectra as a consequence of introducing different number of submicron-sized objects in the buffer and deposited on the sensitive substrate. The size of the objects corresponds to that of large viruses and/or small bacteria. We analyze different geometries. In particular, rectangular, circular and semicircular objects are considered in Sections 3.1.1, 3.1.2 and 3.1.3, respectively. They tend to mimic in a simple way, the geometries of different biological microorganisms [33, 34]. Section 3.2 analyzes the electromagnetic behavior of a large (micron-sized like eukaryotic cells) object on a nanostructured substrate. The flattening effect is analyzed: cells are "flexible objects", they change their morphology when interacting with a substrate [35]. For instance, they spread on its surface when they are deposited on a flat surface. Finally, Section 4 presents the most remarkable conclusions.

2. Theoretical methods

As stated in the introduction, SP's play a basic role in the generation of the EOT phenomenon. SP's can be excited at the dielectric-metal interface and their dispersion equation is given by [36]

$$k_{\text{SP}} = \frac{\omega}{c} \sqrt{\frac{\epsilon_1 \epsilon_2'}{\epsilon_1 + \epsilon_2'}} \tag{1}$$

ω being the frequency of the incident radiation, c the speed of light in vacuum, ϵ_1 the dielectric constant of the dielectric medium and ϵ_2' the real part of the metal dielectric constant. This equation does not consider neither any interactions due to periodicity nor the fact that the metallic substrate is a thin-film.

According to Eq. (1), the SP wave vector is always larger than the wave vector of light in vacuum. Thus, it is not possible to excite SP with photons. There are several ways of providing the necessary extra-momentum using for instance attenuated total reflectance (ATR) couplers, gratings couplers, etc [13, 14, 37–39]. In this paper, a periodic nanohole array is considered to provide the extra-momentum [36]. In fact, the momentum matching condition is given by [40]

$$\mathbf{k}_{\mathrm{SP}} = \mathbf{k}_{||} \pm i\mathbf{G}_x \pm j\mathbf{G}_y \tag{2}$$

$\mathbf{k}_{||}$ being the component of the incident wave vector parallel to the surface of the metallic film, i and j integer numbers corresponding to the different orders of the reciprocal lattice and $\mathbf{G}_x$, $\mathbf{G}_y$ the vectors of the reciprocal lattice, whose modules are: $|\mathbf{G}_x| = |\mathbf{G}_y| = \frac{2\pi}{P}$, where P is the lattice period.

According to Eq. (2), when the periodicity of the lattice is taken into account, Surface Plasmon-Bloch Waves (SP-BW's) appear, whose dispersion relation is given by [8]

$$\lambda_{\mathrm{SP}} = \frac{P\sqrt{\frac{\epsilon_1 \epsilon_2}{\epsilon_1 + \epsilon_2}}}{\sqrt{i^2 + j^2}} \tag{3}$$

Our objective is to analyze the spectral response of a nanostructured system with either submicron- or micron-sized dielectric objects on its surface and immersed in a buffer, so it is necessary to know the SP's penetration depth δ_ϵ within the buffer. This magnitude determines the length scale over which the SP's modes are sensitive to changes in the system buffer + object refractive index. δ_ϵ depends on the wavelength of the incident radiation and the dielectric constants of both the dielectric and metal media [12, 13, 37].

$$\delta_\epsilon \approx \frac{\sqrt{|\epsilon_2'|}\lambda}{2\pi\epsilon_1} \tag{4}$$

Figure 1 shows the penetration depth of SP's in water ($n_{\mathrm{w}} = 1.33$) as a function of the incident radiation wavelength when the metallic medium is made of gold [41]

All the numerical results shown in this research were obtained using COMSOL Multiphysics [42]. Our simulation configuration consists of a periodic nanohole array (hole radius $R = 90\,\mathrm{nm}$) perforated in a gold thin-film (thickness $t = 60\,\mathrm{nm}$) [41]. The period in x and y directions is $P = 500\,\mathrm{nm}$. The selected values for these parameters were chosen according to previous studies for obtaining high sensitivity to changes in the buffer refractive index in the visible spectral region [43, 44]. The nanoarray is located on a glass substrate. Water is implemented as the medium in which the objects are immersed since it reproduces the optical behavior (similar refractive index) of buffer solutions used to keep the pH constant in biological samples. The illumination consists of a plane wave polarized along the x axis and propagating along the z axis (Fig. 2). Figure 2 shows a scheme of the 3D unit cell, which for numerical purposes, is repeated periodically using Bloch conditions [42].

From a computational point of view, the 3D problem is very difficult to solve, mainly due to the very high number of elements necessary to discretize the system (object + substrate). Without loss of generality, in order to overcome this issue, we have transformed the 3D problem into a 2D one as in previous works for solving similar electromagnetic problems [45, 46]. As it is shown later, a comparison of the transmission spectra for 2D and 3D configurations (by keeping fixed the rest of geometrical parameters, period, hole size and film thickness) shows that although
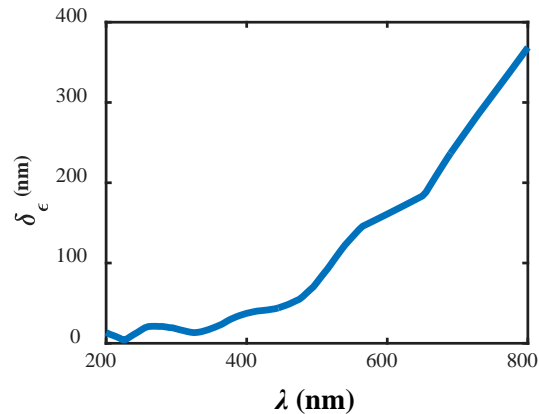
Fig. 1. Penetration depth δ_ϵ of SP's in the dielectric medium (water in this case $n_w = 1.33$). Gold was considered as the metallic material [41].
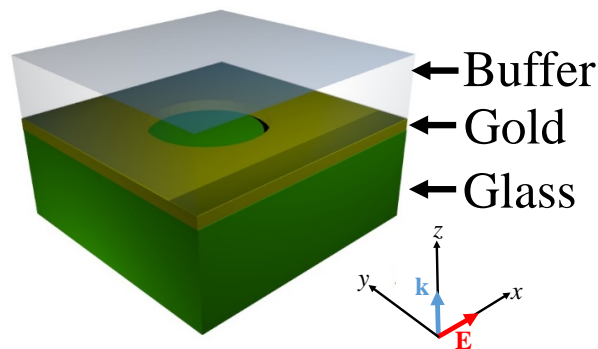

Fig. 2. Scheme of the unit cell used for simulating the periodic nanohole array in 3D. The illumination consists of a plane wave propagating along the z axis and linearly polarized along the x axis. **k** and **E** represent respectively the propagation direction and the polarization of the incident radiation.

quantitative results are different, similar conclusions can be drawn concerning sensitivity in detection. For both configurations, we focus on the analysis of the same EOT resonance. It is due to SP's propagating in the interface water-gold (XZ plane in Fig. 4). When the refractive index of the buffer medium is increased, a spectral red-shift is observed. Furthermore, this shift is higher for a 3D configuration than for a 2D one. Therefore, the sensitivity results shown for the 2D configuration can be considered an underestimation of what will be measured experimentally with a realistic 3D arrangement [47, 48].

Figure 3(a) schematically represents the geometry used in the 2D COMSOL simulations. The periodic array consists of a nanostructured gold thin-film of thickness $t = 60$ nm [41], where nanoapertures of width $W = 180$ nm are perforated. The nanoapertures are filled with air and the period is fixed to $P = 500$ nm. We follow the Cassie and Baxter approach [49]. This assumes that the liquid forms a line of contact on the rough surface with air trapped below the contact line, as opposite to the Wenzel's formulation [49], where the liquid fills up the nanoapertures. This model

has been validated experimentally with similar gold nanoapertures. The gold film is sandwiched between two media: a glass substrate and water as buffer. On top of the gold film, diverse dielectric objects are introduced. Their shape, size and optical properties are changed in order to focus the study on their influence on the transmission spectra. In particular, for submicron-sized objects, changes in the transmission spectra are studied as a function of the number of dielectric objects located on the gold surface. The analysis is carried out for different geometries (rectangles, circles and semicircles). For micron-sized objects, we analyze two different aspects. On one hand, the influence of the number of nanoapertures covered by a circular object due to its flattening effect on the substrate surface. On the other hand, the electromagnetic response of the nanostructured substrate when the refractive index of the object immersed in the buffer is changed. The whole system (constituted by objects, the nanostructured metallic film, the glass supporting substrate and the water buffer) is periodically repeated each 20 μm using Floquet periodicity conditions [42]. The size of the unit cell is large enough to cover the biggest object considered in this work. This structure is illuminated from the glass side with a Gaussian beam polarized along the x axis. The minimum beam waist ω_0 corresponds to 20 μm. The height of the water layer is varied according to the size of the objects inside the buffer. For submicron-sized objects, the chosen height was $H = 500$ nm, whilst for the micron-sized ones, $H = 200$ nm. These values are selected in order to decrease the number of elements for generating the mesh, improving the numerical convergence. In Fig. 3(b), the normalized near field map of the electric field norm ($|\mathbf{E}|$ in linear scale) is shown in the plane XZ at 768 nm (wavelength corresponding to the resonance generated by the SP's at the interface water-gold, see Fig. 4(b)).
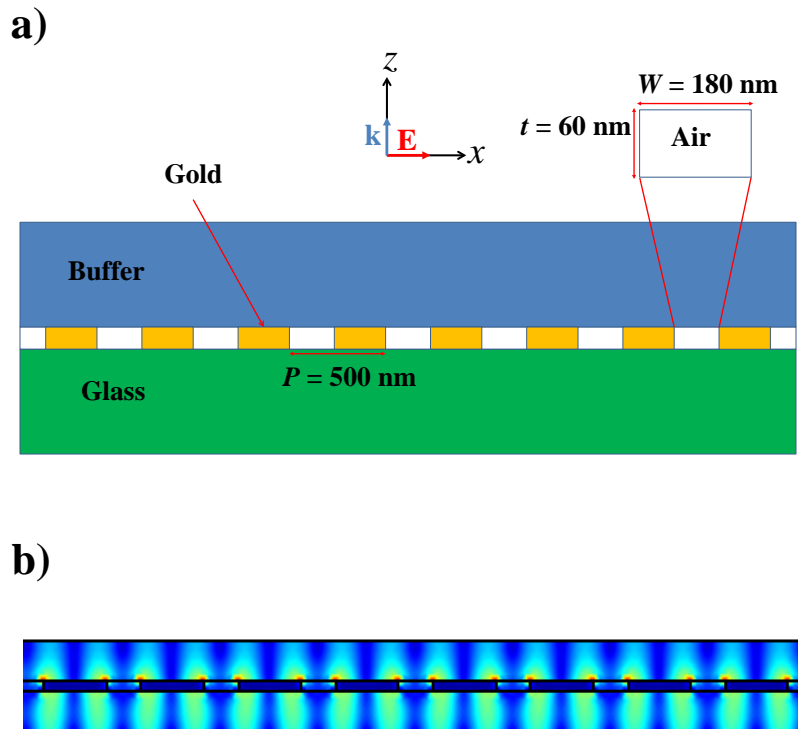
a)

b)

Fig. 3. (a) Scheme of a 2D periodic array. The system is illuminated with a Gaussian beam propagating along the z axis and linearly polarized along the x axis. (b) Normalized near field map of the electric field norm ($|\mathbf{E}|$ in linear scale) in the plane XZ at 768 nm.

In Fig. 4, the transmission spectra for the (a) 3D and (b) 2D configurations described above are shown, considering water as buffer, $n_w = 1.33$. All the results shown in this research correspond to the (1,0) resonance originated by the SP's in the water-gold interface (SP $- n_w$ EOT resonance) centered at ca. 760 nm in both graphs. As it has been previously demonstrated [4, 50, 51] this mode is the most sensitive one to changes in the buffer refractive index. As stated before, the sensitivity is higher for 3D than for 2D configuration (according to our calculations, it reaches values of 374 and 230 nm/RIU, respectively).
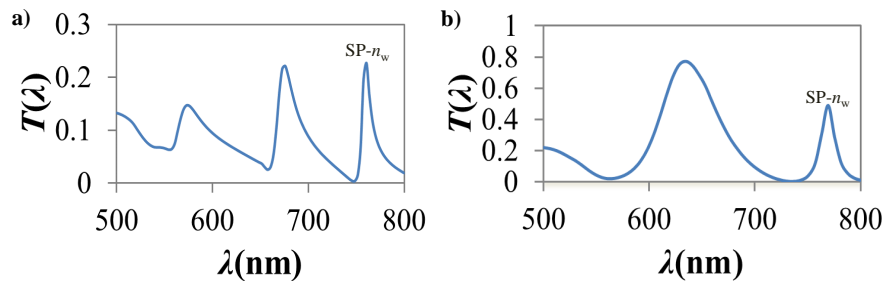
Fig. 4. Transmission spectra of a periodically nanostructured gold thin-film of thickness ($t = 60$ nm) and period ($P = 500$ nm) sandwiched between two dielectric media made of water and glass. (a) 3D geometry (hole radius $R = 90$ nm), (b) 2D geometry (nanoapertures width $W = 180$ nm).

3. Results

We have considered a 2D gold nanostructured thin-film located on a glass substrate in order to analyze its electromagnetic behavior when both small (submicron-sized) and large (micron-sized) dielectric objects are located on it. For the former, we study the electromagnetic response of the nanostructured system when the object size is comparable to the SP's penetration depth in the buffer medium (for instance, large viruses and small bacteria). For the latter, the case where the object is large compared to the penetration depth of the surface plasmon in the buffer is analyzed. This can mimic the cells behavior. We deal with different object shapes. In particular, for the submicron-sized ones, we have chosen rectangles, circles and semicircles, all of them with the same area. Due to the different geometry, the contact surface between the object and the nanostructured substrate, as well as the area of the object inside the plasmon penetration depth in the buffer may be different. The analyzed geometries are intended to mimic the morphology of biological organisms like large viruses or small bacteria. The typical shape of these is cylindrical (many bacteria) or circular (viruses use to have polyhedrical shapes) [33, 34]. Also, more complex geometries can be observed like that of vibrio bacteria which show the shape of a circular ring sector. The rectangular shape is chosen to reproduce the cross-section of a cylindrical microorganism. For this geometry, the entire object inside the SP's penetration depth in the buffer will be considered. Also, the contact surface between the object and the substrate is large. On the contrary, for the circular geometry (simplified shape of typical viruses), only a small fraction of the object is inside the SP's penetration depth in the buffer. The contact surface between the object and substrate is minimal. As an intermediate case, we consider the semicircular geometry, which can model in a first approximation a vibrio-like shape. The object area inside the SP's penetration depth in the buffer is similar to that of the rectangle. However, the contact surface between the object and the substrate is smaller. Our goal is to show the influence of the contact surface. For much larger objects like cells, the flattening effect of a circular object located on the nanostructured substrate is studied. We simulate the cell adhesion to the substrate during the

spreading stage [35]. It can also represent the morphological change suffered by the cell when it is trapped by specific antibodies and attached to the substrate surface. As the flattening of the object increases, the contact surface between the object and the substrate also increases.

3.1. Submicron-sized objects

3.1.1. Rectangular objects

In this section we analyze the influence of rectangular submicron-sized objects on the transmission spectra. Figure 5 shows a scheme of the studied geometry with only one rectangular object. The object area is $0.12 \, \mu m^2$ (width:1200 nm, height: 100 nm), which represents 2.5% of the representative area ($0.24 \times L \, \mu m^2$) within the SP's penetration depth in the water buffer (240 nm), considering that the whole system (particles and metallic nanostructure) is repeated periodically every $L = 20 \, \mu m$ (for clarity, in Fig. 5, L is smaller than $20 \, \mu m$). Such a small area is chosen in order to reproduce a relevant experimental situation in biosensing, where typically the amount of biological material to detect is small compared to the area occupied by the buffer. For this particular geometry, the entire object is inside the plasmon penetration depth in the buffer.
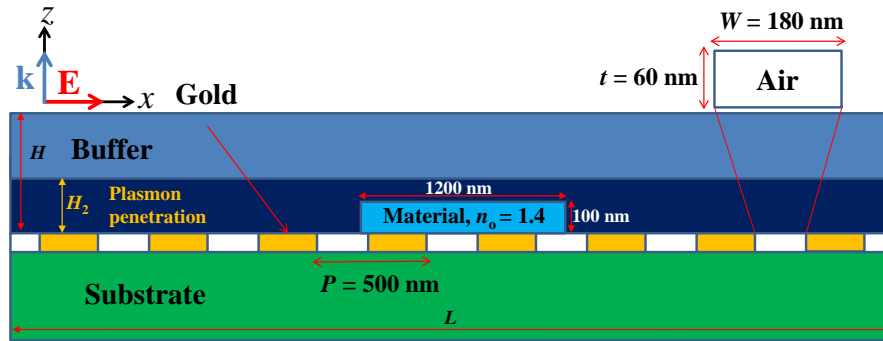

Fig. 5. Configuration of the studied geometry for rectangular objects, which have been placed on the nanostructured substrate described in Section 2. The area of the rectangles is $0.12 \, \mu m^2$ and their refractive index $n_o = 1.4$.

Figure 6(a) shows the transmission spectra of the $SP - n_w$ EOT resonance corresponding to different number of rectangular objects located on the substrate. The changes observed in the spectra are due to the induced change in the effective refractive index because of the presence of these objects. We have quantified the sensitivity of the metallic nanostructured substrate to changes in the number of objects inside the buffer from the spectral shifts observed in the transmission spectra when different number of objects are located on it. The sensitivity is defined as:

$$S_{NO} = \frac{\delta \lambda_{max}}{\delta NO} \tag{5}$$

where NO refers to Number of Objects and λ_{max} is the wavelength corresponding to the maximum value of the transmission spectra.

The number of objects is varied from 1 to 5. Figure 6(b) represents the spectral position of the maximum value in the transmission spectra as a function of the number of objects immersed in the buffer. The sensitivity S_{NO} is $0.56 \, nm/NO$.
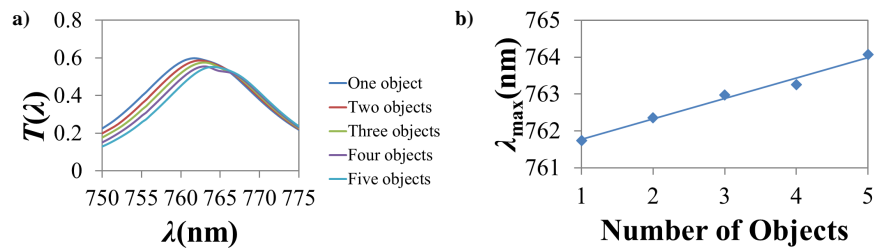
Fig. 6. (a) Transmission spectra of the $SP - n_{\mathrm{w}}$ EOT resonance due to the presence of rectangular objects in the water buffer and located on the nanostructured gold film. (b) Spectral position of the maximum value in the transmission spectra as a function of the number of objects.

3.1.2. Circular objects

In this section, circular objects of radius is $R = 196$ nm are considered. Figure 7 schematically shows the geometry with only one object. Again, for clarity, in Fig. 7, L is smaller than 20 μm.
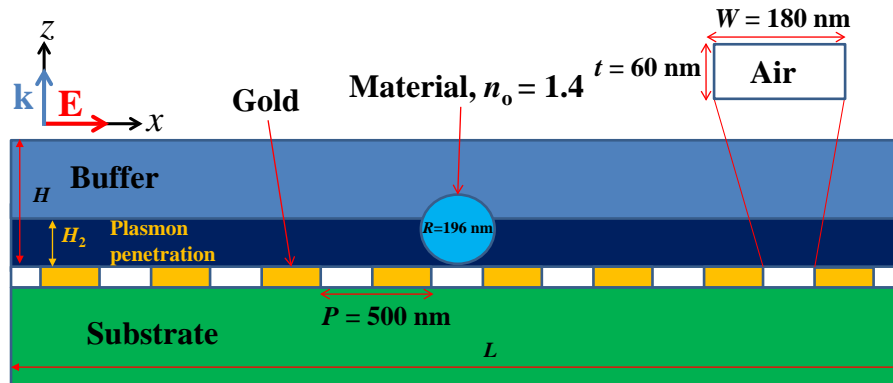

Fig. 7. Configuration of the studied geometry for circular objects. The area of the circles is $0.12 \, \mu m^2$ and their refractive index $n_{\mathrm{o}} = 1.4$.

The transmission spectra of the $SP - n_{\mathrm{w}}$ EOT resonance corresponding to different number of objects located on the nanostructured substrate are shown in Fig. 8(a). As in the previous case, the spectra red shift when the number of objects increases. In Fig. 8(b) we represent the spectral position of the maximum value in the transmission spectra as a function of the number of objects immersed in the water buffer. The obtained sensitivity is 0.19 nm/NO. We observe that the spectral shift caused by such circular objects is almost negligible compared with that corresponding to the rectangular ones. There are two main factors which influence this low sensitivity value: the area of the object inside the plasmon penetration surface is approximately $0.077 \, \mu m^2$ (1.6% of the total effective area, i.e., of the representative area within the SP's penetration depth in the buffer), and the contact between the object and the substrate is through one only point, see Fig. 7. Opposite to this, for the rectangular geometry, the entire object is inside the plasmon effect, covering 2.5% of the total effective area and the object overspreads 1 or 2 nanoapertures, which means that the contact surface between the object and the nanostructured surface is larger than in the case of the circular shape. Thus, the higher sensitivity obtained for rectangular objects compared to the circular ones is mainly due to the object morphology.
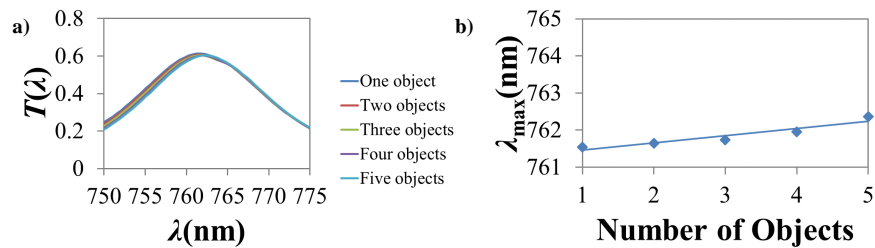
Fig. 8. (a) Transmission spectra of the $SP - n_w$ EOT resonance due to the presence of circular objects in the water buffer and located on the nanostructured gold film. (b) Spectral position of the maximum value in the transmission spectra as a function of the number of objects.

3.1.3. Semicircular objects

The influence of the contact surface between the object and the substrate on the sensitivity values has been analyzed in greater depth by means of semicircular objects (see Fig. 9). Their radius is $R = 277$ nm to keep the same area as the rest of the analyzed geometries in previous sections. For clarity, in Fig. 9, L is smaller than $20\,\mu$m.
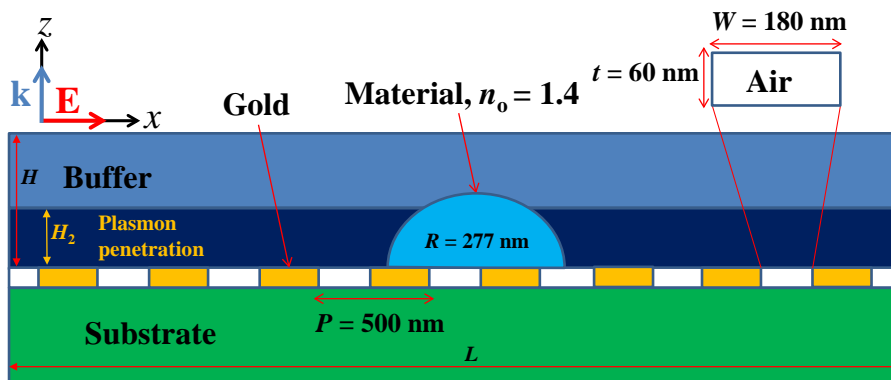

Fig. 9. Configuration of the studied geometry for semicircular objects. The area of the semicircles is $0.12\,\mu m^2$ and their refractive index $n_o = 1.4$.

Figure 10(a) shows the transmission spectra of the $SP - n_w$ EOT resonance, as a function of the number of semicircular objects inside the water buffer. As for the previous geometries, a red shift is observed as the number of inclusions increases. Figure 10(b) represents the wavelengths corresponding to the maximum values of the $SP - n_w$ EOT resonance as a function of the number of objects. The sensitivity obtained in this case is 0.41 nm/NO, which is lower than for the rectangular geometry. In spite of the object area inside the SP's penetration depth in the buffer being similar for both rectangles and semicircles, the sensitivity value is quite different. In fact, a variation of 5% in the object area respect to the effective area of the SP within the buffer gives rise to a 35% variation in the sensitivity values. This means that the different sensitivity can be mainly attributed to the contact surface between objects and substrate, which is larger for the rectangular shape.
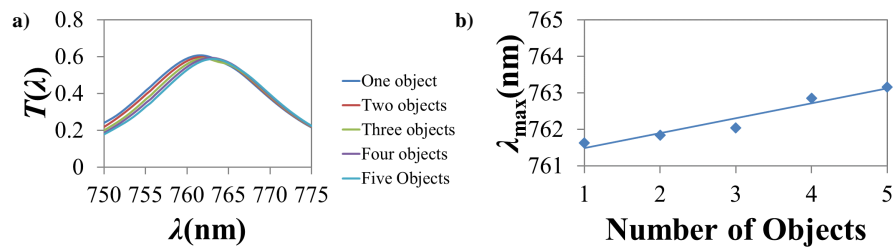
Fig. 10. (a) Transmission spectra of the $SP - n_w$ resonance due to the presence of semicircular objects in the water buffer and located on the nanostructured gold film. (b) Spectral position of the maximum value in the transmission spectra as a function of the number of objects.

3.2. Micron-sized objects. Flattening effects

In this section, we aim to investigate how micron-sized objects (real cells, for instance) with different optical properties and flattening effects on the metallic film surface affect the transmission spectra of the nanostructured substrate.
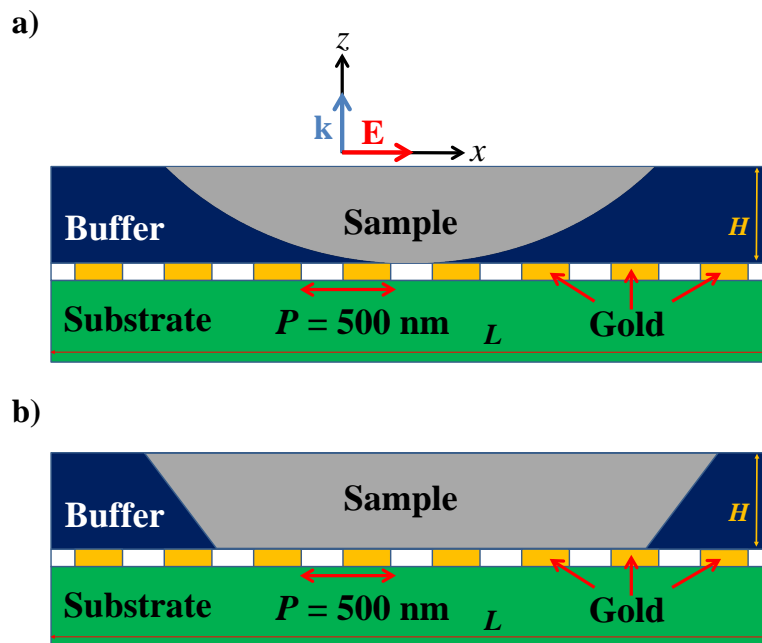

Fig. 11. Configurations used for studying the flattening effect of a large object ($R = 10\,\mu m$) on a nanostructured metallic film substrate. The contact surface between the object and the substrate is (a) through only one point (rigid object) or (b) the object covers some nanoapertures (flexible object like a conventional cell).

We consider a circular object of radius $R = 10\,\mu m$ immersed in the water buffer, as shown in Fig. 11(a). In order to analyze the flattening effect, the shape of the object is modified, thus changing the number of nanoapertures covered by the object (see Fig. 11(b)). The refractive index of the object is $n_o = 1.4$. This is changed from $n_o = 1.33$ to $n_o = 1.45$ with steps of 0.03 to analyze the influence of the optical properties of the micron-sized object. Also, two different flattening configurations are considered: 1) the contact surface between the object and

the nanostructured substrate in through only one point or 2) covering 6 nanoapertures. The height of the water layer is kept to $H = 200\,\text{nm}$. This means that the entire simulated geometry inside that buffer layer is affected by the plasmon effect.

Firstly, we study the morphology effect on the transmission spectra. To this purpose, we consider that the object can be rigid or flexible, which is more realistic from a biological point of view. For a rigid object, the morphology of the object is not affected by the presence of the substrate and consequently, the contact surface between the object and the substrate is through only one point (Fig. 11(a)). However, for flexible objects (cells), due to the substrate presence, a flattening effect may appear. As it was previously introduced, the flattening can be observed during the spreading stage of a cell or when it is trapped by specific antibodies and attached to the substrate surface. As the object is more flexible, the contact surface with the substrate increases. In order to explore this behavior, we have considered that the contact between the circular object of radius $R = 10\,\mu\text{m}$ and the substrate is through a single point or covering 2, 4, 6, 8, 10 or 12 nanoapertures. A red shift is observed in the spectra as the number of covered nanoapertures increases, see Fig. 12(a). In Fig. 12(b), the spectral position of the maximum value in the transmission spectra as a function of the number of nanoapertures blocked by the object is shown. From these results, the sensitivity of the nanostructure (S_{NA}) to changes in the morphology of the object can be obtained. This is defined from the spectral shifts of the $SP - n_{\text{w}}$ EOT resonance as a function of the number of nanoapertures covered by the object

$$S_{\text{NA}} = \frac{\delta\lambda_{\text{max}}}{\delta\text{NA}} \tag{6}$$

where NA stands for the Number of Apertures of the nanostructured substrate blocked by the object.

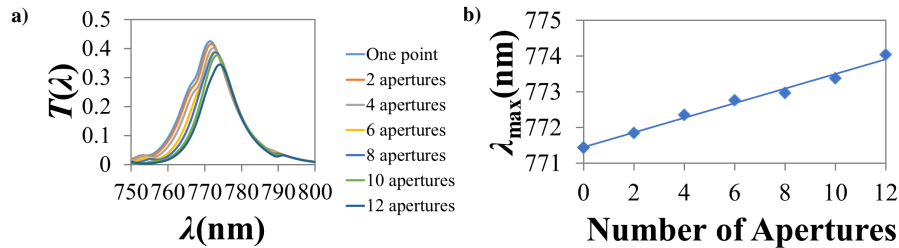The obtained sensitivity value through the Eq. (6) is: 0.21 nm/NA

Fig. 12. (a) Transmission spectra of the $SP - n_{\text{w}}$ resonance due to the presence of a large, circular object ($R = 10\,\mu\text{m}$) in the water buffer and located on the nanostructured gold film for different contact surfaces. (b) Spectral position of the maximum value in the transmission spectra as a function of the number of nanoapertures blocked by the object.

The influence of the object morphology has been clearly demonstrated (see Fig. 12). As the contact surface increases, the resonance red shifts and the transmission value decreases. This behavior is due to the rise of the object area with a higher refractive index than that of the buffer inside the penetration depth of the surface plasmon in water. So, this effect is equivalent to increasing the refractive index of the object while keeping its contact surface with the substrate constant. In order to corroborate this assumption, in Fig. 13 we show the effect of increasing the object refractive index, $n_{\text{o}} \in [1.33, 1.45]$, keeping the same geometry (and hence the same contact surface between the object and the nanostructured substrate). In Fig. 13(a) the contact surface between the object and the substrate is through only one point, whilst in Fig. 13(c) the object blocks 6 nanoapertures. As it is expected from the results analyzed before, spectral shifts appear in both spectra. However, the shifts are higher for the case where the object blocks a larger number of nanoapertures. To validate this, in Figs. 13(b) (the contact surface between the object

and the substrate is through only one point) and 13(d) (the object blocks 6 nanoapertures) we show the wavelengths corresponding to the maximum values of the $SP - n_{\mathrm{w}}$ EOT resonance as a function of the refractive index of the object immersed in the buffer. By means of the slope of the curve, it is possible to obtain the sensitivity of the nanostructured system to changes in the object refractive index, which is given by Eq. (7). The obtained results are $S_{n_{\mathrm{o}}} = 47.1\,\mathrm{nm/RIU}$ and $S_{n_{\mathrm{o}}} 60.6\,\mathrm{nm/RIU}$ for the cases where the contact surface between the object and the substrate is through only one point or the object blocks 6 nanoapertures, respectively.

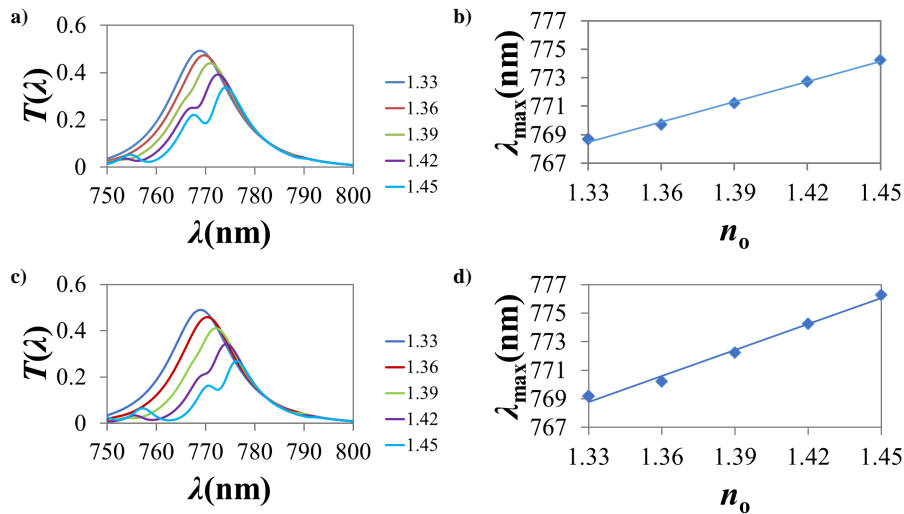$$S_{n_{\mathrm{o}}} = \frac{\delta \lambda_{\mathrm{max}}}{\delta n_{\mathrm{o}}} \tag{7}$$

Fig. 13. Transmission spectra of the $SP - n_{\mathrm{w}}$ resonance due to changes in a micron-sized object refractive index: $n_{\mathrm{o}} \in [1.33, 1.45]$. The contact surface between the object and the substrate is through (a) only one point or (c) the object blocks 6 nanoapertures. In (b) and (d), the wavelength corresponding to the maximum value of the $SP - n_{\mathrm{w}}$ resonance is plotted as a function of the object refractive index when the contact surface between the object and the substrate is through only one point or the object covers 6 nanoapertures, respectively.

It is important to remark that the dependence of the transmitted light spectrum on the refractive index of the object can be used as a sensing tool. It is possible to obtain the object refractive index through the spectral shift of the $SP - n_{\mathrm{w}}$ EOT resonance, given the characteristics of the nanostructured substrate, the refractive index of the buffer and the number of nanoapertures blocked by the object.

4. Conclusions

In this research, we have analyzed the electromagnetic behavior of a metallic thin-film with a periodic array of subwavelength apertures when dielectric objects immersed in a water buffer are located on it. This analysis has been performed for different object sizes, geometries and optical properties. In particular, we have analyzed submicron- and micron-sized objects. This work is inspired by two linked recent interests, that of liquid biopsies for diagnosis purposes and the use of this kind of nanostructured substrates for detecting biological material in low concentrations whose size can go from tens of nanometers (proteins, small viruses, rests of RNA) to hundreds of nanometers (submicron-sized objects, large viruses, small bacteria) or even microns (micron-sized objects, cells).

For submicron-sized objects, we have analyzed the influence of two different aspects on the transmission spectra of the considered nanostructured substrate: On one hand, the area of the object inside the penetration depth of the surface plasmon in the buffer, and, on the other, the contact surface between the object and the substrate. We have compared three basic geometries: rectangles, circles and semicircles. All of them can mimic shapes of a biological microorganisms (bacteria, viruses or eukaryotic cells). For all geometries, we have obtained the sensitivity of the nanostructured substrate to changes in the number of objects located on its surface. The highest (lowest) sensitivity values are observed for the rectangular (circular) geometry. There are two main reasons for this behavior. For the simulated rectangles, the entire object has been chosen to be inside the penetration depth of the surface plasmon in the buffer and the contact surface between the object and the substrate is larger than for the rest of analyzed geometries (rectangles block 1 or 2 nanoapertures). The influence of the contact surface between the object and the substrate has been addressed by means of the comparison between rectangles and semicircles. The area of the object inside the SP's penetration depth in the buffer is almost the same for both geometries. However, the contact surface is larger for the former, which is responsible for the highest sensitivity values. The obtained results suggest some relevant conclusions. The contact surface between the object and the substrate is a critical factor for obtaining high sensitivity values and it is not necessary that the entire object is inside the SP's penetration depth to be detected. This becomes important when the aim of the nanostructured system is intended to detect large objects. In this case, most of the object is outside of the SP's penetration depth in the buffer. In all the cases, when the number of objects inside the buffer increases, a red shift of the analyzed resonance appears due to the increment of the effective refractive index of the medium. This means that it is even possible to count the number of objects (cells for instance) when several of them are on the sensor surface.

For the case of micron-sized objects, the influence of the flattening effect (usual cell geometry evolution when deposited on a flat substrate. This effect can be observed during the spreading stage of a cell or when it is trapped by specific antibodies and attached to the substrate surface) of the object on the substrate has been shown by means of the spectral shifts observed in the transmission spectra. As the cell is flattened, the contact surface between the object and the substrate is increased. As a consequence, the detection of the object can be improved. Larger contact surfaces between the object and the substrate lead to higher sensitivity values. As the flattening increases, the transmission spectra red shift. This behavior is due to the rise of the object area with a higher refractive index than that of the buffer inside the penetration depth of the surface plasmon in water. For that reason, increasing the contact surface between the object and the substrate is equivalent to increasing the refractive index of the object by keeping the same geometry.

Through the obtained results, it is observed that for both small and large objects the sensitivity increases as the area of the object inside the plasmon penetration depth in the buffer increases.

Moreover, the spectral shifts observed when the refractive index of the object changes (keeping the same geometry) can be used as a sensing tool, once the characteristics of the nanostructured substrate, the optical properties of the buffer and the number of nanoapertures covered by the object are fixed. This allows to differentiate healthy cells (their refractive index is around 1.33) from malignant ones (their refractive index is around 1.40) [19, 52]. As a final remark, we believe that the results contained in this research can guide biomedical researchers and experimentalists in the process of detecting and monitoring biological material with large sizes. This has special interest in those biological tests where liquid biopsies are employed.

Funding

Energy and the Environment Program.

Acknowledgments